First principles LDA + U and GGA + U study of protactinium and protactinium oxides: dependence on the effective U parameter

K. O. Obodo[11,*] and N. Chetty[1,21,†]

[11]*Physics Department, University of Pretoria, Pretoria 0002, South Africa;* [2]*National Institute for Theoretical Physics,Johannesburg, 2000, South Africa*

(Dated: February 7, 2013)

The electronic structure and properties of protactinium and its oxides (PaO and PaO_2) have been studied within the framework of the LDA, GGA(PBE), LDA + U and GGA(PBE) + U implementations of density functional theory. The dependence of selected observables of these materials on the effective U parameter has been investigated in detail. The examined properties include lattice constants, bulk moduli, effect of charge density distributions, the hybridization of the 5f orbital and the energy of formation for PaO and PaO_2. The LDA gives better agreement with experiment for the bulk modulus than the GGA for the Pa but GGA give better structural properties. We obtained that PaO is metallic and PaO_2 is a Mott-Hubbard insulator. This is consistent with observations for the other actinide oxides. We discover that GGA and LDA incorrectly give metallic behavior for PaO_2. The GGA(PBE) + U calculated indirect band gap of 3.48 eV reported for PaO_2 is a prediction and should stimulate further studies of this material.

PACS numbers: 61.48.Gh, 68.35.bg, 73.22.Pr

I. INTRODUCTION

Protactinium is the first element in the actinide series with a 5f electron.[1] In some systems (PaO_2, UO_2, NpO_2, PuO_2), the presence of 5f electrons leads to an improper description of the electronic and the structural properties by DFT.[2–7] Several approaches have been developed to overcome these shortcomings of DFT such as the self-interaction correction (SIC), DFT hybrid approach, DFT + U, GW etc. The DFT + U (LDA + U and GGA + U) approach has been shown to effectively correct many of the deficiencies observed by this class of materials with regards to the band gap.[8–10] This approach introduces an on-site Hubbard U and the Hund's J. Dudarev *et al.*[11] combined these two terms in the rotationally invariant formalism to a single term U_{eff}=U−J, referred to as the simplified LSDA + U. The introduction of this *adhoc* parameter leads to a significant improvement in the description of some 5f systems where DFT fails but the choice of the value of this parameter is debatable. The U_{eff} parameter can be obtained: (i) from constrained LDA approach,[8] (ii) from constrained RPA,[12] (iii) from a self-consistent approach,[13] and (iv) from fitting the parameter to experimental observables.[14]

Pa and its oxide are used in scintillators for detecting X-rays, for radioactive dating (determination of ancient artifact), in cathode ray tubes with bright green fluorescence, as high temperature dielectrics for ceramic capacitors, in nuclear weapons (used as support in nuclear chain reactions), etc.[15] These materials have downsides which has limited its study, namely (i) the high toxicity and radioactive nature and (ii) the limited availability. These materials are mainly found as a by-product in nuclear reactions. Furthermore, these materials are (iii) strongly correlated, giving rise to failures by conventional DFT methods.

The understanding of the electronic and structural properties is paramount to harness and control these materials optimally. The elements in the 5f series with localized electrons possess greater atomic volumes and symmetrical structures compared to those with itinerant electrons.[16,17] Hence, Pa exists in the bct, fcc and orthorhombic (α-U) phase at standard temperature and pressure (STP), high temperature and high pressure respectively. Pa metal possesses itinerant 5f electrons with characteristic properties such as superconducting and high vaporization.[15,18,19]

There has been significant interest in the understanding of Pa metal,[20] due to its unique behavior as the first element with a 5f electron. The effect of pressure induced phase transitions has been explored theoretically and experimentally. Haire *et al.*[21] experimentally showed that Pa metal undergoes a pressure induced structural phase transition at 77 GPa from the bct structure (space group *I4/mmm*) to an orthorhombic, α-U structure (space group *Cmcm*) with ∼ 30% atomic volume reduction and no subsequent phase transition. This was predicted by theoretical studies,[16,22] which attribute this to the increase in 5f electron participation in the bonding.

The studies of protactinium oxides (PaO and PaO_2) have been limited to the mode of synthesis and purification for the production of Pa metal.[15] Prodan *et al.*[23] used the density functional hybrid approach to study actinide dioxides and obtained a band gap of 1.4 eV for PaO_2. To the best of our knowledge, no further studies have been performed to shed more light on the electronic structure of PaO_2. Hence, a proper description of the electronic and structural properties of these oxides within the DFT and DFT + U methods is appropriate to understand the physics of these materials.

A systematic first principles study of the dependence of the effective Hubbard-U parameter on LDA + U and GGA + U functionals in Pa and its oxides is lacking. In this work, the DFT methodology is applied to calculate the electronic and structural properties of Pa metal. Using a semi-empirical fit, we then optimize the Hubbard U parameter to give a proper description of PaO and PaO_2. The structural and electronic properties of these oxide materials are determined to investigate the role played by the *5f* electrons.

In Section II, a brief description of the theoretical and com-

putational methodologies is presented. In Section III, the results and discussions for Pa and its oxides are presented, followed by the conclusions in Section IV.

II. THEORY AND COMPUTATIONAL DETAILS

All calculations were performed using density functional theory[24] as implemented in the VASP code.[25] The electron wave functions were described using the projector augmented wave (PAW) method of Blöchl in the implementation of Kresse and Joubert.[26] The LDA[27] and PBE[28] form of the GGA exchange-correlation potentials were used together with their LDA + U and GGA + U variants. An adequately converged kinetic energy cutoff of 500 eV, 500 eV, 550 eV was chosen to ensure fully converged total energies for Pa, PaO and PaO_2 respectively. A spacing of **k**-points of 0.2/Å fine mesh for the Monkhorst-Pack[29] grid is used to sample the Brillouin zone, and Methfessel-Paxton smearing[30] with a width of 0.2 eV was used to integrate the bands at the Fermi level. The total energy, electronic band structure and density of states (DOS) were calculated using the tetrahedron integration method with Blöchl corrections.

Subsequently, we introduce the Hubbard U parameter for the onsite interaction strength. The U parameter was computed by optimizing the lattice parameter with respect to U. This resulted in differences for a range of results involving the physical structure, the electronic structure and the energetics within the GGA and LDA schemes for the oxides. Results presented in this work uses LSDA, GGA, LSDA + U and GGA + U for the oxides but without the U parameter for Pa atom.

A method using the least-squares fit,[31] as implemented in the MedeA-MT module, was used to obtain the elastic constants. This uses the tetrahedron method for the Brillouin zone integrations. The elastic properties were calculated from the Hill values which are a geometric mean of the Voigt and Reuss values. The eigenvalues of the stiffness matrix gives an indication of the mechanical stability of the systems under consideration, which is used to obtain the elastic constants. The Hill values[32] were used in the estimation of longitudinal, shear and mean sound velocities, and the Debye temperatures.[33]

The energy of formation for each structure was calculated by taking the difference between the total energy of the compound (PaO_n) and the energies of its constituents in their corresponding bulk forms:

$$\Delta H_f = E^{tot}_{(PaO_n)} - N_{Pa}\, E^{bulk}_{(Pa)} - N_O\, E^{bulk}_{(O)}\,, \qquad (1)$$

where n is either 1 or 2, N_{Pa} and N_O are the number of Pa atoms and O atoms in the PaO_n compound respectively, $E^{bulk}_{(Pa)}$ is the energy per Pa atom in the bct phase, and $E^{bulk}_{(O)}$ is the energy per O atom in the oxygen molecule.

The phonon calculations were done using the general direct approach of lattice dynamics as implemented in the MedeA-PHONON package.[34]

III. RESULTS AND DISCUSSION

A. Preamble

We carried out self consistent calculations to determine the ground states of Pa and its oxides using spin-polarized (SP) and spin-orbit coupling (SOC) within the DFT + U approach. The inclusion of the effective Hubbard U is excluded for Pa metal because DFT gives a reasonable description of the metal.[16] Pa element is a heavy metal with an atomic number of 91, hence relativistic effects are important. In order to account for the relativistic effects in these systems, the inclusion of SOC is important. In this study, we have shown that in order to obtain the correct properties of PaO_2, the effect of SOC has to be taken into account.

The U parameter in this study is optimized with respect to the lattice constant. The U parameter obtained is used to calculate the structural and electronic properties of the systems. This gives a qualitatively and quantitatively better description of the properties of PaO and PaO_2.

The U parameter accounts for the onsite Coulomb interaction which leads to the localization of the 5f electrons in these systems. In contrast, the standard DFT fails to account for the localization of the electrons, but leads to the delocalization which is a consequence of the Pauli-exclusion principle. The localization of the 5f orbitals leads to a non-magnetic (NM) insulating ground state for PaO_2 but does not change PaO from metallic to insulating.

In order to obtain the correct ground state for PaO_2 for a given U parameter, we lifted the symmetry constraints in the calculations of the electronic and the structural properties allowing the systems to evolve and explore all of phase space, i.e. all stable and metastable phases, including magnetic phases. This has an effect of significantly increasing the computational time as all **k**-points in the Brillouin zone are treated independently, i.e. the special **k**-point set is not reduced by symmetry.

Gryaznov *et al.*,[35] studied UN, UO_2 and PuO_2 with the inclusion of SOC and showed that to correctly describe these systems the lifting of symmetry constraints is absolutely essential. There have been various methodologies proposed by different authors on how to achieve the true ground state within the DFT + U formalism including SOC, such as monitoring the occupation matrix,[36] ramping the Hubbard U parameter,[37] etc. In this study, the symmetry constraints are lifted and the correct ground state is obtained for PaO_2 within the SOC scheme for all the values of U considered. In our work, the symmetry constraints are lifted and the correct ground state is obtained for PaO_2 within the SOC. However, the SP does not yield the correct ground state because relativistic effects are unaccounted for.

B. Crystal structures

Fig. 1 shows the conventional unit cells of Pa, PaO and PaO_2.

Pa has three crystallographic forms which are (i) the body centered tetragonal structure (bct) at STP which transforms to (ii) the face centered cubic structure (fcc) at elevated temperature, and which undergoes a pressure-induced structural transformation to the (iii) α-Uranium structure. The Pa (bct) phase is presented in Fig. 1a.

In Fig. 1b, we present the PaO system which crystallizes in the NaCl structure.

PaO_2 contains antiferromagnetically (AFM) ordered Pa atoms with an underlying fluorite structure that leads to a double tetragonal unit cell (with $c = \sqrt{a}$) when the magnetic ordering is taken into account. The AFM ordered structure is shown in Fig. 1c, where the magnetic ordering is in the z-axis.

C. Structural properties

As indicated earlier, Pa has been observed to exist in various different phases. The STP phase which is the bct structure has experimental lattice parameters of a_0 = 3.925 Å and c = 3.238 Å.[21] LDA is known to underestimate the lattice parameter while GGA generally overestimates the lattice parameter. However, in the early actinides lattice constants obtained using the GGA are found to be better corroborated with experiment compared with the LDA.[38] In Table I, we show our calculated values of the lattice parameters obtained using the GGA and the LDA within the SOC and the SP schemes. Upon complete optimization, the system evolves to a NM ground state consistent with experiment. The lattice parameter, density and volume obtained within the GGA approximation are more comparable to experiment than LDA. As far as the structural properties are concerned, the extension of our methodology to include the Hubbard U parameter is not necessary in the case of metallic Pa.

In Fig. 2, we present the calculated lattice parameter of PaO as a function of the U parameter, where the dotted line indicates the experimental value of a_0. The variation of the lattice parameter is a monotonically increasing function with respect to the U parameter within the SOC and SP scheme. At U= 2.5 eV, the GGA + U (SOC and SP scheme) yields the experimental lattice parameter for PaO. The corresponding result using the LDA + U (SOC and SP scheme) significantly underestimates the lattice parameter. Increasing U to a value of 5.5 eV still does not give a sufficiently accurate result for the lattice parameter within the LDA + U scheme. This shows that the use of the U parameter is better suited within GGA than LDA in the present case. Since a value for U that is too large pushes the f orbitals too far down into the O2p based levels.[39] At U= 0 eV, PaO (within SOC scheme) results in a magnetic ground state. This system evolves with the increase of the U parameter to a NM metallic ground state. This observation is similar to the SP case for the GGA + U. LDA + U gives a NM metallic ground state at all values of the U parameter.

The PaO_2 structure is fully geometrically optimized using the SP and SP + SOC (hence forth referred to as SOC) within the DFT + U. The inclusion of SOC in the fluorite structure of PaO_2 without SP does not transform the structure to the AFM ordered state similar to UO_2. Rather, the inclusion of SP does yield structures which are AFM ordered leading to the symmetry breaking for the PaO_2. For consistency, the structure used in the study is the tetragonally distorted structure obtained when the PaO_2 is in the AFM ordered state. In Fig. 3, the calculated lattice parameter as a function of the U parameter is presented where the dotted line indicates the experimental value. The variation of the lattice parameter is a monotonically increasing function with respect to the U parameter within the SOC and SP schemes. Fig. 3a and 3b shows the variation of a_0 and c_0 respectively as a function of the U parameter. For U = 4.0 eV, the LDA + U with SOC yields a reasonable lattice parameter (5.501 Å) which is approximately equal to the experimental value (5.509 Å), compared to the LDA + U with SP, which grossly underestimates lattice parameter. On the other hand, for U = 2.0 eV, the GGA + U with SOC gives a slightly higher (about 0.8 %) lattice parameter for PaO_2 and only slightly underestimates (about −1.01 %) the lattice parameter using the SP scheme. With this value for U we go on to evaluate all further properties of interest for this PaO2.

Our conclusions for PaO_2 about the accuracy of GGA over LDA within the DFT + U schemes are similar to those for PaO.

D. Elastic properties

We find Pa to be elastically stable due to the absence of negative elastic constants. In Table I, we present the theoretical and experimental bulk modulus for Pa. There are discrepancies between previously reported theoretical[38] and experimental[40,41] values for the bulk modulus of Pa. In these previous studies, the value of the experimental bulk modulus obtained was found to be high compared to the theoretical value. These discrepancies were suggested to result from (i) the presence of a small amount of hard martensitic phase not detectable using X-rays and/or (ii) the presence of large experimental errors in the early diamond anvil cell techniques.[20] Recent experimental studies by Haire *et al.*[21] obtained a bulk modulus of 118.00 GPa. This value is lower than previously reported experimental results. In our study using LDA with SOC, the bulk modulus is found to be 117.93 GPa which compares excellently with the reported experimental value. The bulk modulus obtained using GGA with SOC is 98.18 GPa, which is slightly lower than the experimental value shown in Table I.

The elastic properties of PaO using GGA and GGA + U (SOC scheme) is presented in Table II. The elastic constants obtained for PaO are all positive definite, hence PaO is elastically stable. But the value of the c_{44} elastic constant for PaO within GGA and GGA + U using the SOC approach is very low compared to the other elastic constants. We calculated the elastic constants for NM and SP cases. The c_{44} elastic constant obtained using NM and SP is also very low compared to the other elastic constants. This is an indication that the material will readily yield to shear stresses. The Debye temperature (Θ_D) is calculated to determine the stiffness of the system. The Θ_D for PaO is 275.4 K.

The elastic constants obtained for PaO_2 are all positive definite. Hence, the PaO_2 structure is elastically stable within GGA and GGA + U as presented in Table III. The elastic properties obtained using GGA are less than those using LDA. This is also consistent with the GGA + U and LDA + U. This is expected because the value of the lattice parameter is higher within the GGA than those obtained using the LDA. The Debye temperature for PaO_2 is 409.5 K. This material is stiff and suggestive of covalent and ionic character. We conclude that PaO_2 is significantly stiffer compared to PaO. The bonding character is fully analyzed in the next subsection.

E. Valence charge densities of PaO and PaO_2

The computed valence charge density using the GGA + U optimized structures (SOC scheme) is presented to elucidate the bonding characteristics and crystal structures of PaO and PaO_2. The computed charge density distribution plot for PaO and PaO_2 is in the (100) plane. The electron density is indicated by the color scale on the side (blue is devoid of electrons and red indicates a high concentration of electrons). The charge densities plotted pertain to the valence states only, summed over both spin directions.

In the PaO crystal structure, the Pa^{2+} ion is almost devoid of valence electrons and the cloud of electrons around O^{6+} ion is almost the full eight electrons needed to give O^{2-} (conventional oxygen is lacking two electrons). The valence charge density for PaO is calculated at U = 2.5 eV, which is determined to be the optimum U parameter for this structure. In Fig 7, it is clearly seen that PaO is characterized by a high spherical charge density distribution around the Pa and O ions and a low charge density in the interstitial region. Compared to the charge density in the interstitial region, relatively high density bridges are present between the atomic spheres. These bridges are an indication of weak covalent bonding between Pa and O atoms due to hybridization of oxygen 2p states with partially occupied Pa f and d states. Therefore, PaO is strongly ionic and weakly covalently bonded.

In the AFM PaO_2 crystal structure, the valence charge density is calculated at U = 2.0 eV, which is determined to be the optimum U parameter for this structure. In Fig. 8, it is clearly seen that PaO_2 is characterized by high spherical charge density distribution around the Pa and O ions with a low charge density in the interstitial region. Compared to the charge density in the rest of the interstitial region there is a low presence of charge density bridges present between the atomic spheres. These bridges are an indication of weak covalent bonding between Pa and O atoms due to hybridization of oxygen 2p states with partially occupied Pa f and d states. The charge density around the Pa atom in PaO_2 structure is low compared to the PaO structure. This is an indication of stronger ionic character in AFM PaO_2 and weak covalent character compared to PaO system. Therefore, PaO_2 is predominantly ionic with significant insulating behavior.

Also, in Table IV, the f occupation for PaO_2 compared to PaO gives credence to the notion that PaO_2 is more ionic.

F. Band structure and density of states

The computed band structure and density of states (DOS) presented below is within GGA + U. The result obtained using LDA + U (with a large value of U) gives qualitatively similar results to GGA + U.

In Fig. 4, we present the band structure and density of states of Pa metal calculated using GGA within the SOC scheme. The band structure and DOS clearly shows that Pa is metallic. The metallicity is largely determined by the Pa-f electrons and a slight contribution from Pa-d electrons, while the Pa-s and Pa-p electrons contribute to the deep lying states.

Fig. 5 shows the band structure of PaO_2 with an indirect band gap of 3.48 eV which is calculated using GGA + U within the SOC scheme at U = 2.0 eV. The LDA + U within the SOC scheme at U = 2.0 eV underestimates the band gap, while the SP scheme within the DFT + U results in a metallic system. The valence band maximum for PaO_2 using GGA + U within the SOC scheme at U = 2.0 eV is located in between the Z-point (0.0 0.0 0.5) and the A-point (0.5 0.5 0.5). While, the conduction band minimum is located at the R-point (0.0 0.5 0.5). In Table VI, the effect of tuning the U parameter on the band gap is tabulated. Increasing the U parameter leads to opening of the band gap at U = 2.0 eV. Subsequently, increasing the U parameter leads to a decrease in the band gap, which is accompanied by a change in the position of the conduction band minimum and valence band maximum.

The DOS for the PaO system using GGA + U is presented in Fig. 9.We find that PaO using various exchange correlation functionals (GGA and LDA) and inclusion of the U parameter is a metallic system. The states around the Fermi level is dominated by the 5f-electrons, which effectively determine the metallicity of the PaO system as shown in Fig. 9. The partial density of states as a function of change in the effective U parameter for the SOC and SP schemes provides an insight on the hybridization and magnetic nature of the system. In the SOC scheme, the PaO system undergoes hybridization and evolves from a magnetic ground state at U = 0 eV with total magnetization of 0.47 μ_B to a NM metallic ground state as a function of U. In the SP scheme, the PaO system undergoes hybridization and evolves from a magnetic ground state at U= 0 eV with total magnetization of 0.51 μ_B to a NM metallic ground state as a function of the U. This is consistent with its neighboring oxides ThO and UO. This observation for PaO with respect to GGA is consistent with LDA, hence the figures and data on LDA are not presented.

The electronic structure of the early actinides dioxides (AO_2, where A=Th, Pa, U, Np) all show insulating character.[23] The ground state of UO_2 and NpO_2 show varying degrees of magnetism, while ThO_2 is NM. These characteristics of U and Np are attributed to the partially occupied 5f electrons, which favors itinerancy for the early actinides. The PaO_2 system within the standard LDA and GGA approach (with SP or/and SOC scheme) is a metallic NM ground state. The inclusion of the Hubbard U parameter leads to band gap opening for the system using the SOC scheme (for GGA and LDA). Because the SOC splits the orbitals, thus allowing for a U induced orbital polarization that opens a gap. However,

the U parameter does not lead to band gap opening using the SP scheme due to the negligence of relativistic effects. In the SOC and SP schemes, the coupling between the Pa ($5f$ and $6d$) electrons and the O ($2p$) electrons is important as presented in Fig. 11.

As mentioned in the preamble, PaO_2 is a difficult system to study computationally due to the subtle nature of the electron correlation for this system. The DOS for an energy cutoff of 400 eV and 550 eV is shown in Fig. 10 and 11 to buttress this point. The lattice parameter of PaO_2 is fully converged as a function of the energy cutoff at 500 eV. Hence, a less converged energy cutoff (400 eV) and a fully converged energy cutoff (550 eV) are used to show the sensitivity of the U parameter. At an energy cutoff of 400 eV, tuning the U parameter leads to significant change in the band gap from 0.3 eV at U = 3.0 eV to 1.37 eV at U = 5.5 eV. At an energy cutoff of 550 eV, the converged U = 2 eV results in a band gap of 3.48 eV. Further tuning of the U parameter leads to a decrease in the band gap, which is shown in Table VI. The band gap obtained for U= 5.5 eV at an energy cutoff of 400 eV is consistent with the study by Prodan *et al.* and recently by Wen *et al.*[39] using the HSE hybrid exchange-correlation functional. Using U = 2.0 eV at a converged energy cutoff of 550 eV, the band gap obtained is 3.48 eV. This value is intermediate to that of ThO_2 (6.2 eV) and UO_2 (2.0 eV) which is consistent with the trend because it shows the onset of $5f$ electron occupation. The Pa $5f$ electrons determine the conduction band maximum and play a significant role in the electronic properties of these systems. The Pa f electrons are localized and result in insulating behavior. This corroborates other results where the crystal structure and the volume of actinides exhibit different bonding configurations.[17]

G. Energy of formation of PaO and PaO_2

The energy of formation for the oxides is calculated using equation 1. The total energy of the constituent elements is deducted from the total energy for the system (PaO or PaO_2). In Table V, we present the energy of formation for the oxides using the LDA + U and GGA + U within the SOC and SP schemes. The calculated energy of formation for PaO and PaO_2 using SOC is lower than that obtained with SP within the DFT + U (LDA and GGA). This implies that the SOC case is more energetically favorable than the SP case. The formation for PaO and PaO_2 is exothermic. This indicates that metallic Pa will oxidize in the presence of oxygen. The energy of formation of PaO_2 is lower than that of the PaO. The implication is that PaO readily oxidizes in the presence of oxygen to form the more energetically favorable di-oxide. Our theoretical results is in line with experimental observation, that the oxides are more favorable than the parent metal and that PaO_2 is more stable than PaO in the presence of oxygen.[15]

H. Phonon studies of PaO and PaO_2

The phonon dispersion for Pa, PaO and PaO_2 is calculated within the GGA (PBE) scheme. The lattice dynamics studies is not carried out for both the LDA and DFT + U scheme. This is because, the inclusion of U parameter does not lead to significant changes in the phonon frequency of these systems. The phonon dispersion calculated exploits the linearity relationship between the induced forces on the atoms in the crystal and the displacement of the atoms from their equilibrium position, which holds within the harmonic regime.

In Fig. 6a, no negative phonon modes for Pa are observed in the phonon dispersion plot, hence this structure is dynamically stable. The maximum frequency for the acoustic modes is about 4.5 THz due to the large mass of Pa atom which does not undergo significant perturbation.

In Fig. 6b, no negative phonon modes for PaO are observed in the phonon dispersion plot, hence this structure is dynamically stable. The low lying frequency modes are governed by the dynamics of heavy Pa atoms. The higher frequencies, on the other hand, are governed by the dynamics of the oxygen atoms which are much lighter compared to Pa atoms. The difference in the frequency of oxygen atoms compared to the Pa atoms is rather large. This suggests that instability in the system can arise from a small perturbation of the crystal structure.

In Fig. 6c, no negative phonon modes for PaO_2 are observed in the phonon dispersion plot, hence this structure is dynamically stable. The low lying frequency modes are governed by the dynamics of heavy Pa atoms, whereas the higher frequencies are governed by the dynamics of lighter oxygen atoms. The difference in the frequency of oxygen atoms compared to the Pa atoms is lower compared with PaO. This implies that the extra oxygen atom has led to the stabilization of the structure.

IV. CONCLUSIONS

The structural, mechanical and electronic properties of Pa have been studied within the DFT method. Inclusion of SP and SOC give an adequate description of this system. As far as the structural properties are concerned, the inclusion of the Hubbard U parameter is not relevant here. We determined that Pa is elastically and dynamically stable.

The structural, mechanical and electronic properties of PaO have been studied within the DFT + U approximation. The inclusion of SP and SOC gives an adequate description of this system. Our calculations show that the properties of this system can be described accurately with an effective U parameter of 2.5 eV within the GGA + U. The results using LDA + U were unsatisfactory. PaO is dynamically stable as shown by the phonon dispersion data. PaO is also stable to isotropic stress because of its positive bulk modulus. However, PaO has a low shear modulus. The charge density plot shows the presence of strong ionic bonding in this system. We conclude that PaO structure will readily oxidize to PaO_2 structure, which is

the more stable form. This is in line with observed experimental results.

The SOC inclusion together with the Hubbard U parameter is essential for the accurate determination of the total energy, electronic and magnetic properties of PaO_2. Within the LDA + U (SOC scheme) at U = 4.0 eV, the lattice parameter is 5.501 Å, which is approximately equal to the experimental result. However, the results for the band gap and the energy of formation are found to be unsatisfactory within this scheme. On the other hand, within the GGA + U (SOC scheme) at U = 2.0 eV, the lattice parameter is 5.553 eV, which is approximately 0.78 % above the experimental value. Within this scheme we derive accurate results for the electronic, elastic and mechanical properties of the system. This method predicts PaO_2 as an insulator with a band gap of 3.48 eV.

Hence, to obtain an accurate description of the PaO and PaO_2, we have shown that the inclusion of the Hubbard U parameter is paramount. In general, the GGA is better suited for the incorporation of the Hubbard U parameter for these systems.

ACKNOWLEDGMENTS

This work is supported by the University of Pretoria. We gratefully acknowledge Material Design Inc. support in particular Rene Windiks, Walter Wolf, Paul Saxe and the members of the Computational and Theoretical Physics group at the University of Pretoria. Also, we are thankful to Dr. Jannie Pretorius for help with the use of the computational resources. NC is grateful to the National Institute for Theoretical Physics for support.

* Kingsley.Obodo@up.ac.za
† Nithaya.Chetty@up.ac.za

[1] Moore Kevin T., van der Laan Gerrit. Nature of the $5f$ states in actinide metals. *Rev. Mod. Phys.*, 81(1):235–295, 2009.
[2] M.S.S.S. Brook, G. Calestani, J.C. Spirlet, J. Rebizant, W. Muller, J. M. Fournier, and A. Blaise. f-Electron Contribution to Bonding in Protactinium Compounds. *Physica B*, 102B:84–87, 1980.
[3] Alexander B. Shick, Vaclav Janis, and Peter M. Oppeneer. Effect of Coulomb Correlations on the Electronic Structure of PuCoGa5. *Physical Review Letters*, 016401(January):1–4, 2005.
[4] Christoph Loschen, Javier Carrasco, Konstantin Neyman, and Francesc Illas. First-principles LDA+U and GGA+U study of cerium oxides: Dependence on the effective U parameter. *Physical Review B*, 75(3):1–8, January 2007.
[5] Bao-tian Wang, Hongliang Shi, Weidong Li, and Ping Zhang. First-principles LDA + U and GGA + U study of neptunium dioxide. *Physical Review B*, 81:3–8, 2010.
[6] M. Fhokrul Islam and Asok K. Ray. A LDA + U study of the photoemission spectra of the double hexagonal close packed phases of Am and Cm. *Solid State Communications*, 150(19-20):938–942, 2010.
[7] Per Söderlind, G. Kotliar, K. Haule, P. M. Oppeneer, and D. Guillaumont. Computational modeling of actinide materials and complexes. *MRS Bulletin*, 35(November):883–889, 2010.
[8] Vladimir I. Anisimov, Jan Zaanen, and Ole K. Andersen. Band theory and Mott insulators: Hubbard U instead of Stoner I. *Physical Review B*, 44(3):943–954, 1991.
[9] A. I. Liechtenstein, V. I. Anisimov, and J. Zaanen. Density-functional theoy and strong interactions: Orbital ordering in Mott-Hubbard insulators. *Physical Review B*, 52(8):5467–5471, 1995.
[10] V. I. Anisimov, F. Aryasctiawan, and A. I. Lichtenstein. First-principles calculations of the electronic structure and spectra of strongly correlated First-principles calculations of the electronic structure and spectra of strongly correlated systems : the LDA + U method. *Journal of Physics: Condensed Matter*, 767:767–808, 1997.
[11] S. L. Dudarev, G. A. Botton, S. Y. Savrasov, C. J. Humphreys, and A. P. Sutton. Electron-energy-loss spectra and the structural stability of nickel oxide: An LSDA + U study. *Physical Review B*, 57(3):1505–1509, 1998.
[12] F. Aryasetiawan, M. Imada, A. Georges, G. Kotliar, S. Biermann, and A. I. Lichtenstein. Frequency-dependent local interactions and low-energy effective models from electronic structure calculations. *Physical Review B*, 70(19):195104, 2004.
[13] Matteo Cococcioni and Stefano De Gironcoli. Linear response approach to the calculation of the effective interaction parameters in the LDA+ U method. *Physical Review B*, 71:1–16, 2005.
[14] G. W. Chinthaka Silva, Philippe F. Weck, Eunja Kim, Charles B. Yeamans, Gary S. Cerefice, Alfred P. Sattelberger, and Kenneth R. Czerwinski. Crystal and Electronic Structures of Neptunium Nitrides Synthesized Using a Fluoride Route. *Journal of The American Chemical Society*, 134:3111–3119, 2012.
[15] Lester R. Morss, Norman M. Edelstein, and Jean Fuger. *The Chemistry of the Actinide and Transcatinide Elements*. 2010.
[16] P. Soderlind. Theory of the crystal structures of cerium and the light actinides. *Advances in Physics*, 47(6):959–998, 1998.
[17] R. G. Haire. Insights into the bonding and electronic nature of heavy element materials. *Journal of Alloys and Compounds*, 445(2007):63–71, 2008.
[18] R. D. Fowler, B. T. Matthias, L. B. Asprey, H. H. Hill, J. D. G. Lindsay, C. E. Olsen, and R. W. White. SUPERCONDUCTIVITY OF PROTACTINIUM *Physical Review Letters*15(22): 860862, 1965.
[19] J. E.Gordon, H. Montgomery, R. J. Noer, G. R. Pickett, and R. Tobon. Superconductivity of Thorium and Uranium *Physical Review*152(1): 432437, 1966.
[20] Hubert Blank. Experimental results on properties of Pa revisited. *Journal of Alloys and Compounds*, 343:108–115, 2002.
[21] R. Haire, S. Heathman, M. Idiri, T. Le Bihan, A. Lindbaum, and J. Rebizant. Pressure-induced changes in protactinium metal: Importance to actinide-metal bonding concepts. *Physical Review B*, 67(13):1–10, April 2003.
[22] Per Soderlind and Olle Eriksson. Pressure-induced phase transitions in Pa metal from first-principles theory. *Physical Review B*, 56(17):10719–10721, 1997.
[23] Ionut D. Prodan, Gustavo E. Scuseria, and Richard L. Martin. Covalency in the actinide dioxides: Systematic study of the electronic properties using screened hybrid density functional theory. *Physical Review B*, 76(033101):1–4, 2007.
[24] P. Hohenberg and W. Kohn. Inhomogeneous Electron Gas. *Physical Review*, 136(3B):864, 1964.
[25] G. Kresse and J. Furthmüller. Efficient iterative schemes for ab initio total-energy calculations using a plane-wave basis set. *Physical Review B*, 54(16):11169, October 1996.

[26] G. Kresse and D. Joubert. From ultrasoft pseudopotentials to the projector augmented-wave method. *Physical Review B*, 59(3):11–19, 1999.

[27] J. P. Perdew and Alex Zunger. Self-interaction correction to density-functional approximations for many-electron systems. *Physical Review B*, 23(10):5048–5079, 1981.

[28] John P. Perdew, Kieron Burke, and Matthias Ernzerhof. Generalized Gradient Approximation Made Simple. *Physical review letters*, 77(18):3865, October 1996.

[29] Hendrik J. Monkhorst and James D. Pack. Special points for Brillouin-zone integrations. *Physical Review B*, 13(12):5188, 1976.

[30] M. Methfessel and A. T. Paxton. High-precision sampling for Brillouin-zone integration in metals. *Physical Review B*, 40(6):3616, 1989.

[31] Yvon Le Page and Paul Saxe. Symmetry-general least-squares extraction of elastic data for strained materials from ab initio calculations of stress. *Physical Review B*, 65:104104, February 2002.

[32] R. Hill. The elastic behaviour of a crystalline aggregate. *Proceedings of the Physical Society, Section A*, 65(5):349, 1952.

[33] Orson L. Anderson. A Simplified method for calculating the Debye temperature from elastic Constants. *Journal of Physics: Chemucak Solids*, 24:909–917, 1963.

[34] K. Parlinski, Z. Q. Li, and Y. Kawazoe. First-Principles Determination of the Soft Mode in Cubic ZrO 2. *Physical Review Letters*, 78(21):4063–4066, 1997.

[35] Denis Gryaznov, Eugene Heifets, and David Sedmidubsky. Density functional theory calculations on magnetic properties of actinide compounds. *Physical chemistry chemical physics : PCCP*, 12(38):12273–8, October 2010.

[36] Boris Dorado, Bernard Amadon, Michel Freyss, and Marjorie Bertolus. DFT + U calculations of the ground state and metastable states of uranium dioxide. *Physical Review B*, 235125(79):1–8, 2009.

[37] B. Meredig, A. Thompson, H. A. Hansen, and C. Wolverton. Method for locating low-energy solutions within DFT+U. *Physical Review B*, 82:2–6, 2010.

[38] P. Soderlind, O. Eriksson, and B. Johansson. Electronic properties of f metals using the generalized gradient approximation. *Physical Review B*, 50(11):7291–7294, 1994.

[39] Wen X.-D. , Martin, R. L., Roy L. E., Scuseria G. E., Rudin S. P., Batista E. R., McCleskey T. M., Scott B. L.,Bauer E. , Joyce J. J., and Durakiewicz T. Effect of spin-orbit coupling on the actinide dioxides AnO2 (An=Th, Pa, U, Np, Pu, and Am): a screened hybrid density functional study. *The Journal of chemical physics*, 137 (15):154707.

[40] Borje Johansson and Hans L. Skriver. Electronics Structure of the Actinide Metals. *Journal of Magnetism and Magnetic Materials*, 29:217–229, 1982.

[41] U. Benedict, J. C. Spirlet, C. Dufour, I. Birkel, W. B. Holzapfel, and J. R. Peterson. X-RAY DIFFRACTION STUDY OF PROTACTINIUM METAL TO 53 GPa. *Journal of Magnetism and Magnetic Materials*, 29:287–290, 1982.

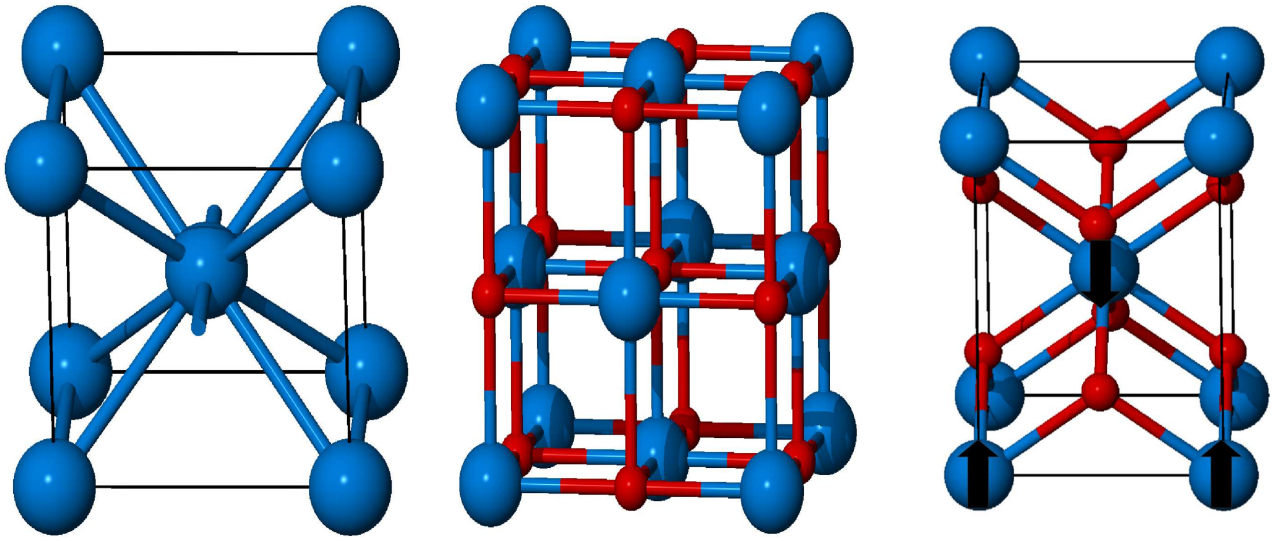

(a) Pa (b) PaO (c) PaO_2

FIG. 1: (Color online) The crystallographic unit cells of (a) Pa, (b) PaO (c) PaO_2. Blue spheres depict Pa and the red spheres depict the oxygen atoms. The black arrows illustrate the AFM ordering in the z-axis

TABLE I: Calculated and experimental lattice parameters in Å, density in g/cm^3, volume in $Å^3$ and bulk modulus in GPa for Pa metal.

Type of calculation	a_0	c	ρ	volume	bulk Modulus
Experiment (Ref. 17)	3.925	3.238	15.382	24.99	118.00
LDA (SOC)	3.815	3.104	16.978	22.75	117.93
LDA (SP)	3.833	3.108	16.805	22.83	115.24
GGA (SOC)	3.907	3.185	15.778	24.32	98.18
GGA (SP)	3.930	3.196	15.543	24.68	94.06

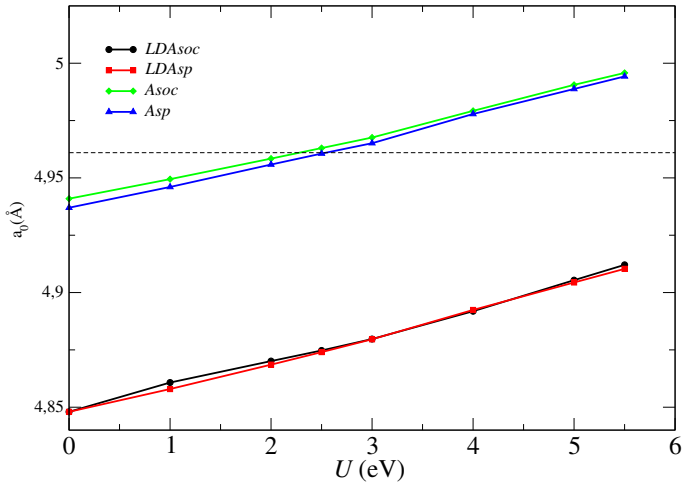

FIG. 2: (Color online) The change in the lattice parameters is plotted within the description of DFT + U (GGA, LDA) approximations for PaO. The U - parameter results in a significant change in the structural parameters.

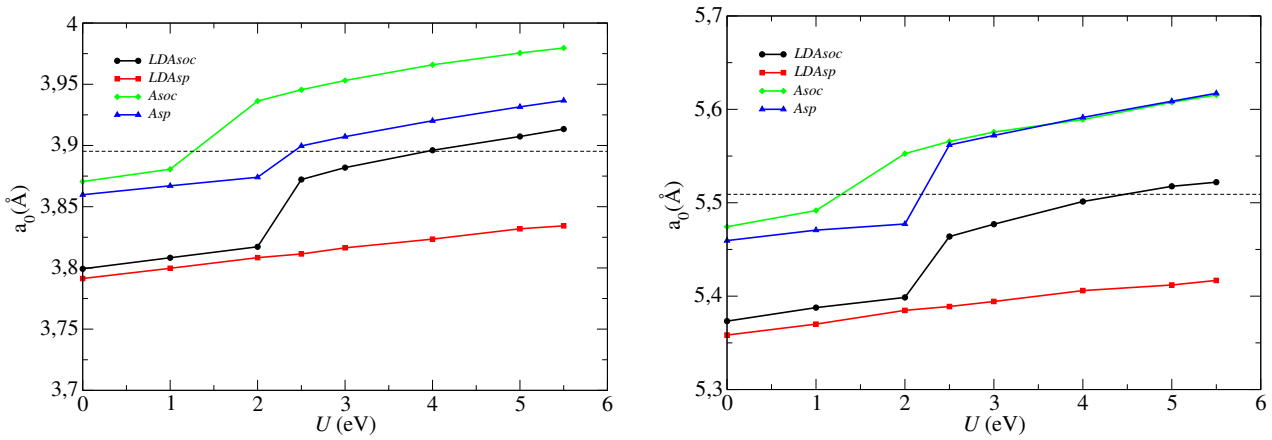

(a) change in a-axis as a function of U - parameter

(b) change in c-axis as a function of U - parameter

FIG. 3: (Color online) The change in the lattice parameters is plotted within the description of DFT + U (GGA, LDA) approximations for PaO_2. It shows that the U-parameter leads to a change in the structural parameters.

TABLE II: Elastic constants, bulk and shear in GPa, Debye temperature in K for PaO. PaO results presented are for the SOC case and the U parameter is 2.5 eV.

Type of Calculation	c_{11}	c_{12}	c_{44}	*bulk*	*shear*	Θ_D
GGA	348.61	106.75	9.08	187.37	34.11	216.5
GGA + U	363.98	92.19	27.57	182.79	55.69	275.4

TABLE III: Elastic constants, bulk modulus and shear modulus in GPa, Debye temperature in K for PaO_2. The PaO_2 results presented corresponds to the SOC and U = 2.0 eV

Type of Calculation	c_{11}	c_{12}	c_{13}	c_{33}	c_{44}	c_{66}	*bulk*	*shear*	Θ_D
GGA	316.96	156.15	103.69	369.93	80.34	132.98	192.32	98.45	421.9
GGA + U	297.93	141.76	99.41	343.81	73.11	123.83	180.09	91.09	409.5

TABLE IV: Partial 5f occupation for Pa, PaO and PaO_2 systems using GGA with SOC.

System	U	5f
Pa	0	1.327
PaO	2.5	1.228
PaO_2	2	1.414

TABLE V: The calculated Energy of formation (eV) for PaO and PaO_2 using LDA + U and GGA + U within the SOC and SP scheme.

Compound	U_{eff}	LDA(SOC)	LDA(SP)	GGA(SOC)	GGA(SP)
PaO	2.5	−6.19	−3.89	−5.43	−3.19
PaO_2	2.0	−12.60	−10.30	−11.62	−8.93

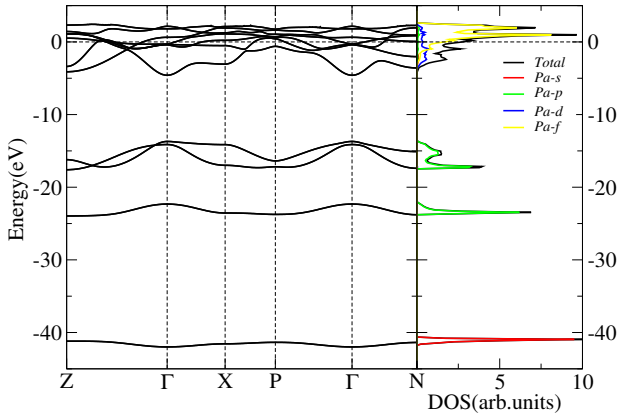

FIG. 4: (Color online) The calculated band structure and DOS plot of Pa in the full Brillouin zone.

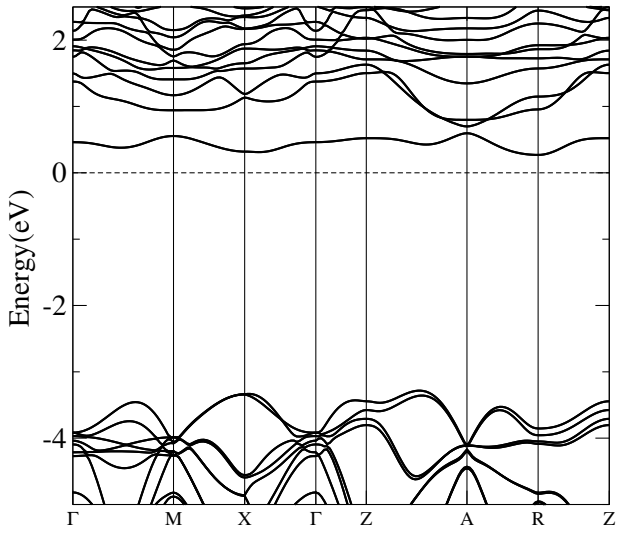

FIG. 5: (Color online) The calculated band structure plot of PaO_2 using DFT + U (U = 2.0 eV) in the full Brillouin zone with an AFM structure. The system contains two unique Pa atoms due to the spin configuration and the O atoms are same.

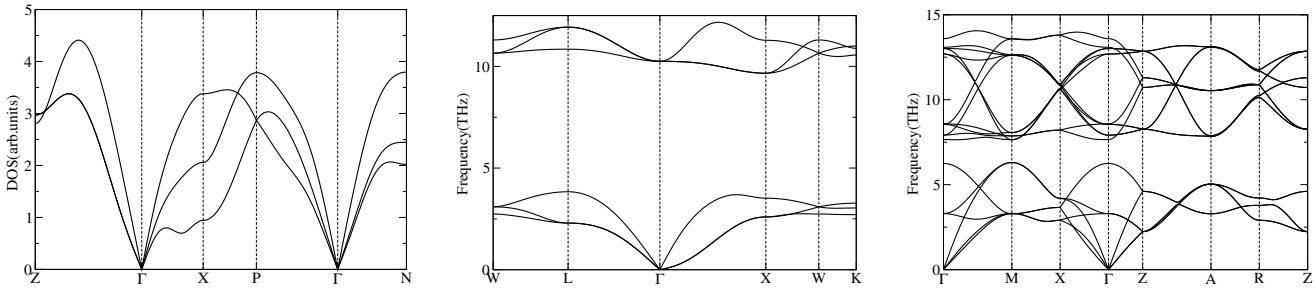

(a) Phonon dispersion of Pa (b) Phonon dispersion of PaO (c) Phonon dispersion of PaO_2

FIG. 6: (Color online) The phonon dispersion plot of PaO and PaO_2, showing the lattice dynamics of Pa and O atoms.

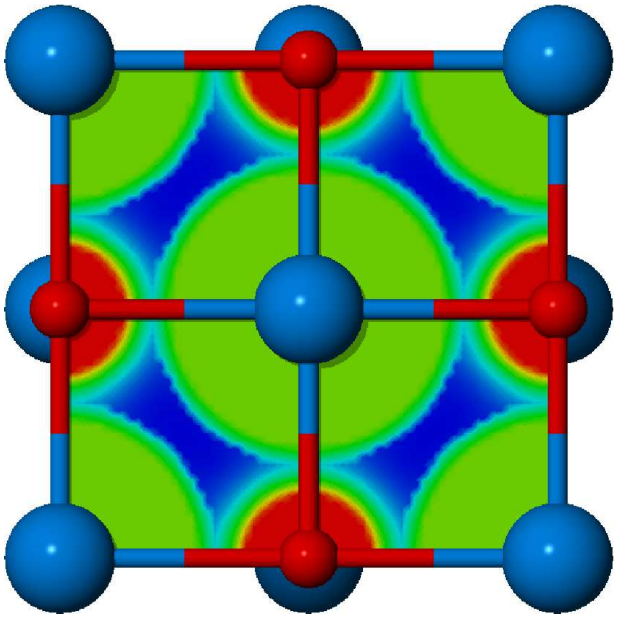

FIG. 7: (Color online) The color pattern of the calculated valence charge density distribution for PaO in the (100) plane, where the blue spheres depict Pa atoms and the red spheres depict the O atoms.

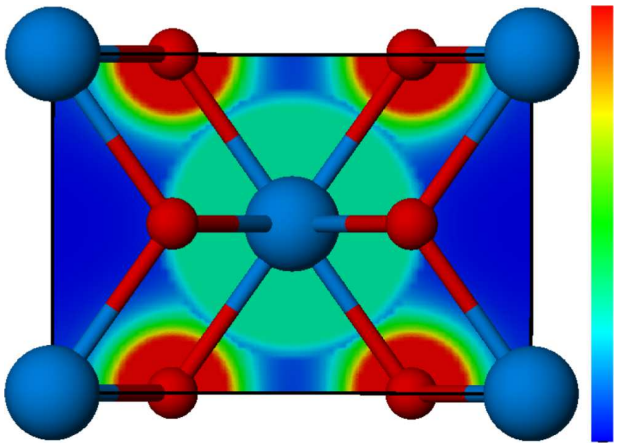

FIG. 8: (Color online) The color pattern of the calculated valence charge density distribution for PaO_2 in the (001) plane, where the blue spheres depict Pa atoms and the red spheres depict the O atoms. The color scale: deep blue color represents low valence charge while the red color represents high concentration valence charge.

TABLE VI: The optimum U parameter as a function of band gap (null band gap indicates a metal) for PaO_2. Where Z (0.0 0.0 0.5), A (0.5 0.5 0.5), R(0.0 0.5 0.5), X (0.0 0.5 0.0), and Γ (0.0 0.0 0.0)

U	Band gap	Position of Band gap	
		Valence Band	Conduction Band
0.0	0.00	–	–
1.0	0.00	–	–
2.0	3.48	in between Z and A	R
2.5	3.40	in between Z and A	in between R and X
3.0	3.30	in between Z and A	in between X and Γ
4.0	3.01	in between Z and A	Γ
5.0	2.72	in between Z and A	Γ
5.5	2.55	in between Z and A	Γ

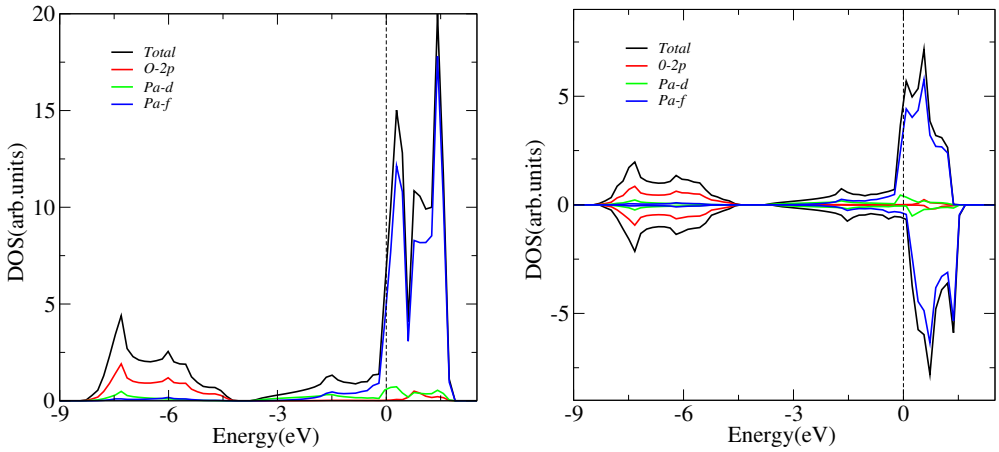

(a) SOC U = 0 (b) SP U = 0

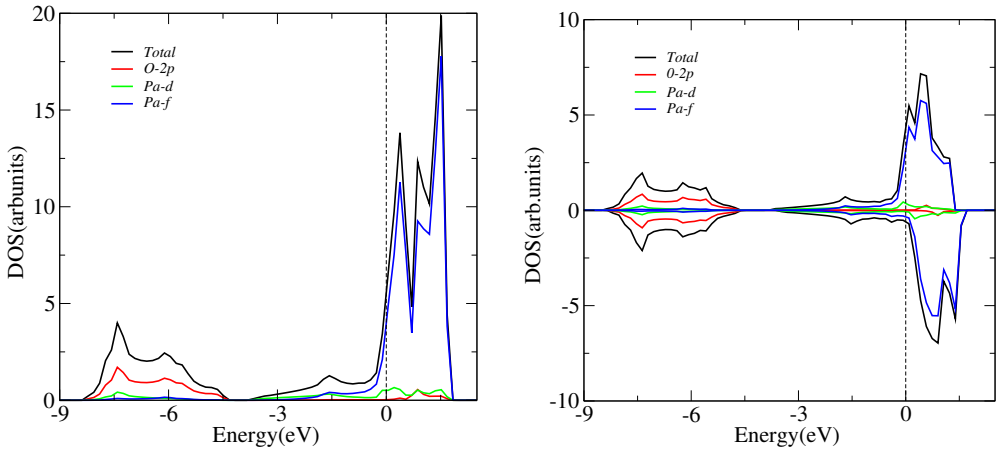

(c) SOC U = 1 (d) SP U = 1

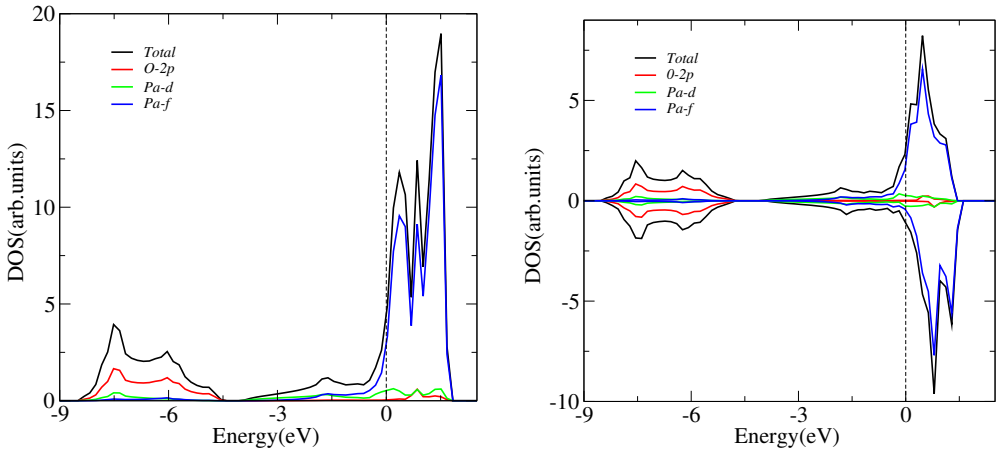

(e) SOC U = 2.5 (f) SP U = 2.5

FIG. 9: (Color online) The total and projected densities of states (DOS) for the spin polarized and spin-orbit coupling of PaO within the descriptions of GGA and GGA + U approximations . All the DOS are calculated at the optimized geometry for the given density functional and magnetic ordering. The Fermi energy level is set at zero and is represented using dashed line. It contains one Pa atoms and the O atoms are same.

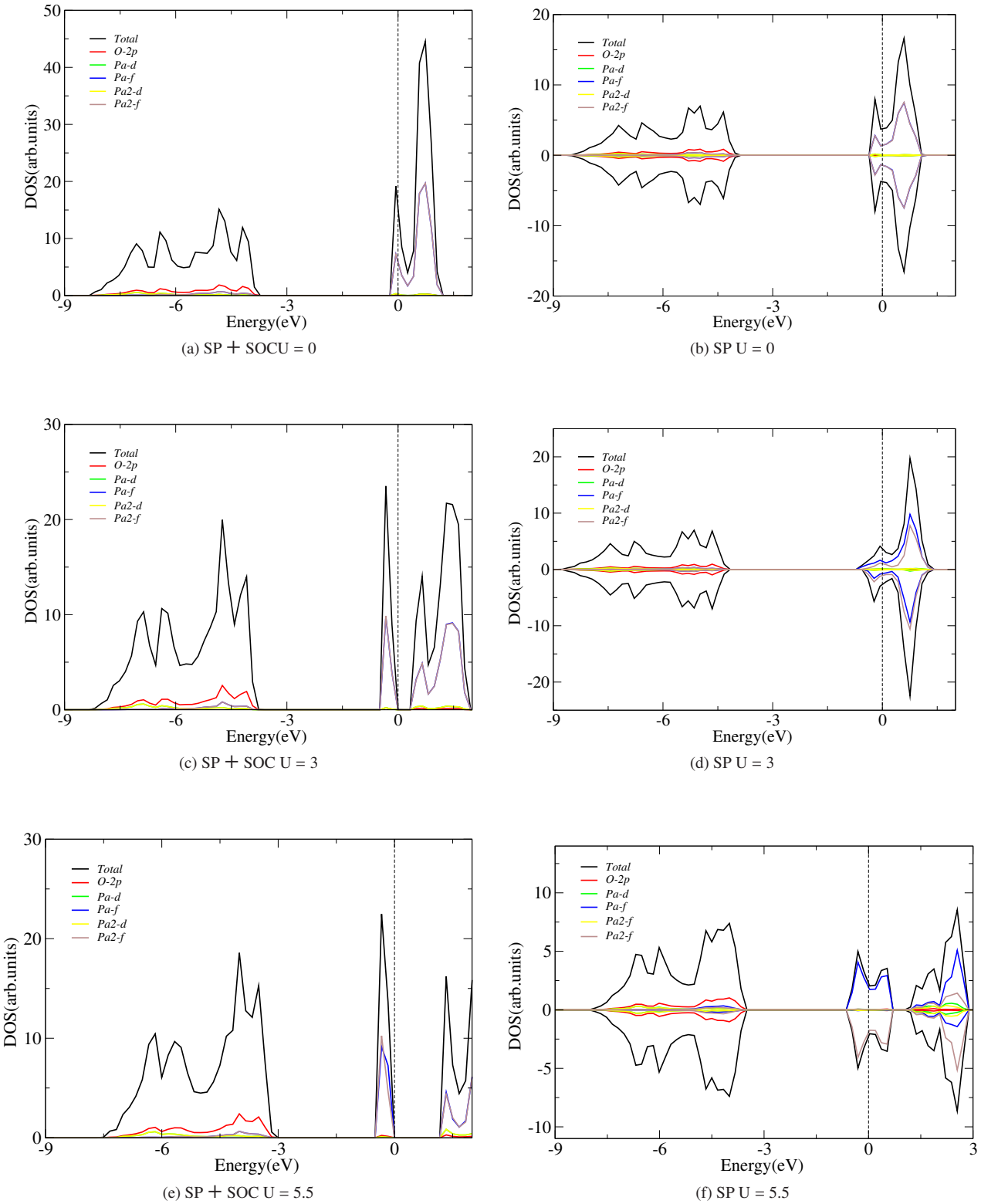

(a) SP + SOCU = 0

(b) SP U = 0

(c) SP + SOC U = 3

(d) SP U = 3

(e) SP + SOC U = 5.5

(f) SP U = 5.5

FIG. 10: (Color online) The total and projected densities of states (DOS) for the SP and SP + SOC of PaO_2 in the AFM ordered phase within the descriptions of GGA and GGA + U approximations at an energy cutoff of 400 eV. All the DOS are calculated at the optimized geometry for the given density functional and magnetic ordering. The Fermi energy level is set at zero and is represented by the dashed line. It contains two unique Pa atoms (label Pa_1 and Pa_2) due to the spin configuration and the O atoms are same.

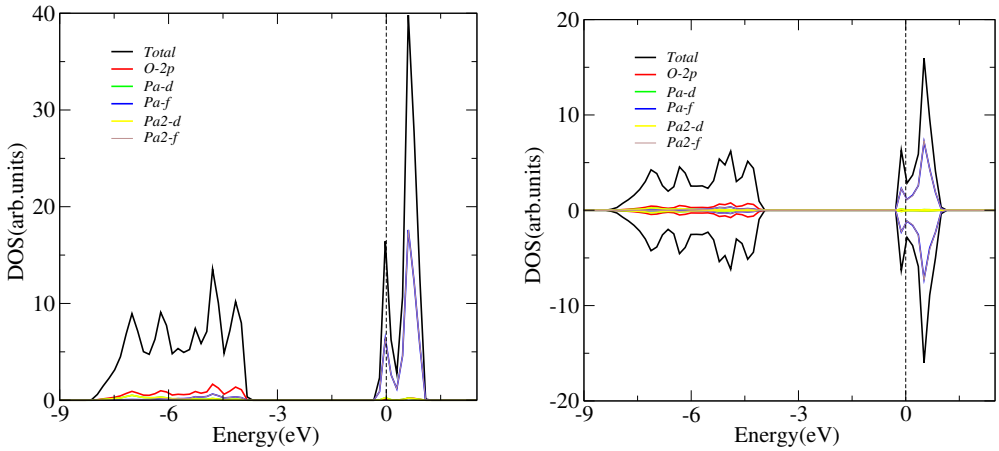

(a) SP + SOC U = 0

(b) SP U = 0

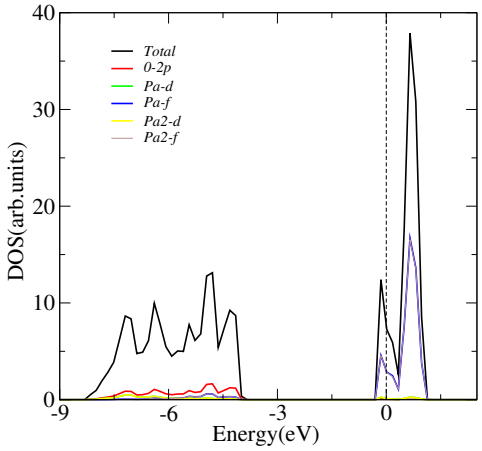

(c) SP + SOC U = 1

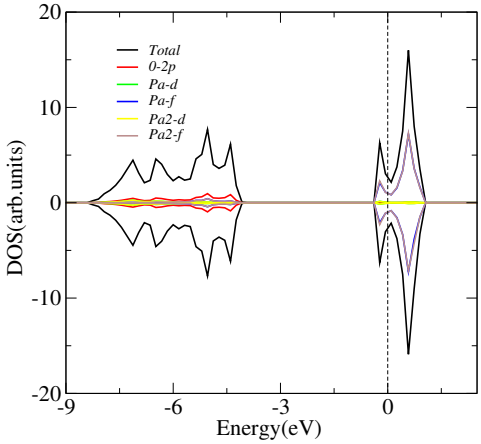

(d) SP U = 1

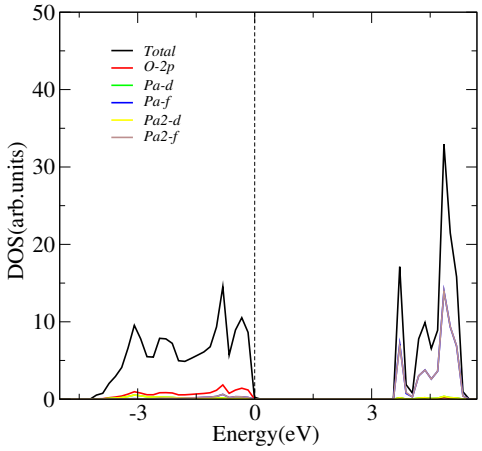

(e) SP + SOC U = 2

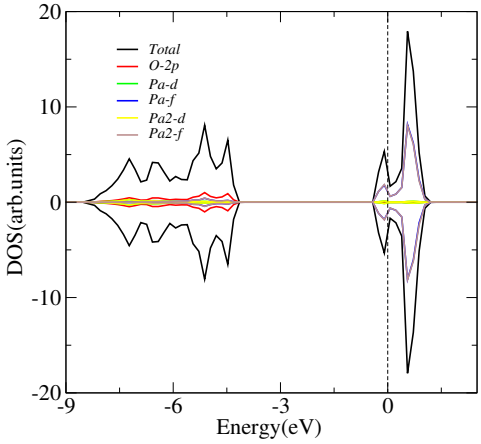

(f) SP U = 2

FIG. 11: (Color online) The total and projected densities of states (DOS) for the SP and SP + SOC of PaO_2 in the AFM ordered phase within the descriptions of GGA and GGA + U approximations at an energy cutoff of 550 eV. All the DOS are calculated at the optimized geometry for the given density functional and magnetic ordering. The Fermi energy level is set at zero and is represented by the dashed line. It contains two unique Pa atoms (label Pa_1 and Pa_2) due to the spin configuration and the O atoms are same.